Spray evaporation model sensitivities

By Shashank, E. Knudsen AND H. Pitsch

1. Motivation and objective

The energy density of solid- and liquid-phase fuels is significantly higher than the energy density of gas-phase fuels. Vehicles with space or weight constraints therefore generate power using multi-phase combustion processes. If these processes are to be simulated for the purpose of engine design and optimization, fuel evaporation must be modeled. Evaporation descriptions are needed regardless of whether the dense fuel phase is dealt with using a Lagrangian method or an Eulerian method. Faeth (1987) and Sazhin (2006) review a variety of modern evaporation models, as well as the assumptions that are invoked in their derivation. The literature in these reviews addresses the modeling problem from a variety of perspectives. For example, Law & Law (1976) test several approaches for calculating the thermodynamic property values that are needed in spray models. Miller *et al.* (1998) test a series of different expressions for the mass transfer number that appears in the evaporation rate. Whereas studies such as these incorporate detailed thermodynamic and fluid physics, the problem of evaporation modeling nevertheless continues to be challenging. This challenge is attributable to the multi-scale and multi-physics processes that influence evaporation: turbulent mixing, combustion, heat transfer, phase change, and interfacial dynamics. Resolution alone cannot be used to address the challenge because these processes remain several orders of magnitude too expensive to fully resolve using typical industrial computational resources. The assumptions that are invoked in the derivation of modern spray models are therefore unavoidable in computationally tractable simulations of engineering devices.

Recently, LES studies of multi-phase combustors have begun to emphasize that critical simulation outputs such as pollutant predictions are very sensitive to the details of evaporation modeling. For example, simulations of NASA's lean direct injection burner (Knudsen & Pitsch 2010) have shown that changes in a spray evaporation model can lead to order-of-magnitude changes in predicted CO and NO_x concentrations. These sensitivities inevitably lead modelers to tune spray coefficients before they are employed in design-oriented engine simulations.

The goal of this study is to better understand the sensitivities of spray evaporation models so that these sensitivities can be accounted for in a modeling framework. One question in particular is considered: which parts of the evaporation modeling framework represent the largest sources of uncertainty? A better understanding of the answer to this question will enable continued LES spray model development. To address this issue, widely used evaporation models such as those of Miller *et al.* (1998) and Sazhin (2006) will be used to simulate a series of single drop evaporation experiments. These simulations build on studies such as those of Hubbard *et al.* (1975) in which sensitivities to reference temperature mixing rules were considered.

The paper is organized as follows. This section serves as an introduction. In section 2, a spray evaporation model framework is introduced. Section 3 then describes two single-drop evaporation experiments that are used as test cases. A series of test simulations

that span a test parameter space are outlined in section 4. Sections 5 through 7 discuss the results of these test simulations, and their implications for spray model advancement. A brief summary of the work is provided in section 8.

2. Spray model description

Spray evaporation models are evaluated in the context of a standard Lagrangian drop tracking framework. In the cases described below only a single drop is simulated. The equations that are solved to describe the drop's position ($x_{d,i}$), velocity ($u_{d,i}$), temperature (T_d), and mass (m_d) are (Miller *et al.* 1998; Miller & Bellan 1999; Okong'o & Bellan 2004)

$$\frac{d}{dt}\left(x_{d,i}\right) = u_{d,i}, \tag{2.1}$$

$$\frac{d}{dt}\left(u_{d,i}\right) = \dot{u}_{d,i} = \frac{f_1}{\tau_d}\left(\widetilde{u}_i - u_{d,i}\right), \tag{2.2}$$

$$\frac{d}{dt}\left(T_d\right) = \dot{T}_d = \frac{\mathrm{Nu}}{3\mathrm{Pr}}\frac{C_p}{C_L}\frac{f_2}{\tau_d}\left(\widetilde{T}_g - T_d\right) + \frac{\dot{m}_d L_v}{m_d C_L}, \tag{2.3}$$

$$\frac{d}{dt}\left(m_d\right) = \dot{m}_d = -\frac{\mathrm{Sh}}{3\mathrm{Sc}}\frac{m_d}{\tau_d}\ln\left(1 + B_M\right). \tag{2.4}$$

Here the i index corresponds to a particular Cartesian direction, the liquid drop's latent heat of vaporization is L_v, and its specific heat is C_L. Quantities that describe the gas surrounding the drop are the filtered flow velocity $\widetilde{u}_i$, the representative ambient gas temperature $\widetilde{T}_g$, and the representative specific heat C_p. τ_d in Eq. (2.4) is a particle time constant defined as $\tau_d = \rho_d d_d^2/(18\mu_r)$ where ρ_d is the density of the drop. d_d is the drop diameter, and μ_r is a representative viscosity associated with the surrounding gas. The correction factor f_1 is a function of the drop's slip Reynolds number,

$$\mathrm{Re}_{d,sl} = \frac{\rho_d d_d}{\mu_r}\left(\left(\widetilde{u}_1 - u_{d,1}\right)^2 + \left(\widetilde{u}_2 - u_{d,2}\right)^2 + \left(\widetilde{u}_3 - u_{d,3}\right)^2\right)^{1/2}, \tag{2.5}$$

and is modeled as (Crowe *et al.* 1998)

$$f_1 = 1 + 0.15\mathrm{Re}_{d,sl}^{0.687} + \frac{0.0175\mathrm{Re}_{d,sl}}{1 + (4.25\times 10^{-4})\mathrm{Re}_{d,sl}^{-1.16}}. \tag{2.6}$$

The f_2 correction factor is (Miller & Bellan 1999)

$$f_2 = \beta/(\exp(\beta) - 1), \quad \beta = \frac{-1.5\ \mathrm{Pr}\ \dot{m}_d\ \tau_d}{m_d}. \tag{2.7}$$

Pr and Sc are the non-dimensional Prandtl and Schmidt numbers, respectively, associated with the gas surrounding the drop. The Nusselt and Sherwood numbers are

$$\mathrm{Nu} = 2 + 0.552\ \mathrm{Re}_{d,sl}^{1/2}\ \mathrm{Pr}^{1/3}, \quad \mathrm{Sh} = 2 + 0.552\ \mathrm{Re}_{d,sl}^{1/2}\ \mathrm{Sc}^{1/3}. \tag{2.8}$$

Drop evaporation in Eq. (2.4) is modeled using the mass transfer (Spalding) number B_M. This quantity is defined

$$B_M = \frac{Y_{d,s} - \widetilde{Y}_f}{1 - Y_{d,s}}, \tag{2.9}$$

where $\widetilde{Y}_f$ describes the mass fraction of fuel in the gas phase surrounding the drop. $\widetilde{Y}_f$ is

filtered and represents an average over the computational cell in which the drop resides. $Y_{d,s}$ is the mass fraction of gas-phase fuel at the drop's surface. A frequently used model form for $Y_{d,s}$ is (Faeth 1987; Nakamura *et al.* 2005; Miller *et al.* 1998)

$$Y_{d,s} = \frac{W_f X_{d,s}}{W_f X_{d,s} + W_g(1 - X_{d,s})}, \tag{2.10}$$

$$X_{d,s} = \frac{P}{P_{atm}} \exp\left(L_v \left(\frac{1}{T_{b,atm}} - \frac{1}{T_{d,s}} \right) \left(\frac{W_f}{R} \right) \right), \tag{2.11}$$

where $X_{d,s}$ is the mole fraction of gas-phase fuel at the drop surface, and where W_g and W_f are the molecular weights of the surrounding gas and fuel, respectively. Equation (2.11) is based on the Clausius-Clapeyron equation, $T_{b,atm}$ is the boiling temperature of the liquid fuel at atmospheric pressure, R is the universal gas constant, and $T_{d,s}$ is the gas phase fuel temperature at the drop surface. P is the pressure and P_{atm} is the reference atmospheric pressure.

To close the evaporation model, the unknown gas phase surface temperature $T_{d,s}$ must be specified. Two models for this quantity will be considered. The first model assumes that the gas phase surface temperature ($T_{d,s}$) can be set equal to the drop's temperature in the liquid phase, T_d. This model is invoked in many DNS and LES spray studies (Miller *et al.* 1998; Reveillon & Vervisch 2005; Baba & Kurose 2008).

Other methods of modeling $T_{d,s}$ can be developed by introducing additional physics. For example, a second model that is considered is derived by defining a second transfer number B_T using energy considerations (Faeth 1987; Sazhin 2006),

$$B_T = \frac{C_p \left(\widetilde{T}_g - T_{d,s} \right)}{L_v + C_L \left(T_{d,s} - T_d \right)}. \tag{2.12}$$

The flux of mass and the flux of energy at the drop surface are consistent in the derivation of the drop model equations only if the transfer numbers B_T and B_M are related. This relationship should be a function of fuel properties. For example, when B_M from Eq. (2.9) is related to the expression for B_T in Eq. (2.12), the following expression is found (Sazhin 2006),

$$\left(1 + \frac{Y_{d,s}(T_{d,s}) - \widetilde{Y}_f}{1 - Y_{d,s}(T_{d,s})} \right)^{\phi} = 1 + \frac{C_p \left(\widetilde{T}_g - T_{d,s} \right)}{L_v + C_L \left(T_{d,s} - T_d \right)}. \tag{2.13}$$

Here $Y_{d,s}$'s dependency on the drop's gas phase surface temperature has been explicity denoted as $Y_{d,s}(T_{d,s})$, and the ϕ parameter in the exponent depends on the specific heats of the ambient and fuel gases, $\phi = C_{p,f}/(C_{p,g}\mathrm{Le})$. Le is the Lewis number in the ambient gas. If the specific heats of the ambient gas and the fuel are assumed to be equal and the ambient Lewis number is taken to be one, the expression reduces to

$$\frac{Y_{d,s}(T_{d,s}) - \widetilde{Y}_f}{1 - Y_{d,s}(T_{d,s})} = \frac{C_p \left(\widetilde{T}_g - T_{d,s} \right)}{L_v + C_L \left(T_{d,s} - T_d \right)}. \tag{2.14}$$

Equations (2.13) or (2.14) can be iteratively solved to find the $T_{d,s}$ associated with a drop. Once known, $T_{d,s}$ can be used to determine B_M in Eq. (2.4).

In the remaining sections the evaporation model which assumes the gas phase drop surface temperature ($T_{d,s}$) and liquid drop temperature (T_d) are equal is treated as the baseline model. This approach is nearly equivalent to the 'M7' model studied by Miller *et al.* (1998), but differs in that the non-equilibrium modification to $X_{d,s}$ is not used in

the present study. This modification was determined to have a negligible effect at the conditions of the experiments that are considered here.

In the simulations shown below, the Navier-Stokes equations are solved to describe the gas-phase fluid around the drop. The width of each gas-phase computational cell is always more than four times as large as the drop diameter. The spray related source terms that appear in the gas phase transport equations can be defined using the solutions of the spray ODE's from Eqs. (2.1)-(2.4). The source term that appears in the continuity and the fuel mass fraction transport equation is $\overline{\dot{\omega}}_{S1} = -\dot{m}_d/V_\Delta$, where the local mesh cell volume is V_Δ. The source term in the momentum equation is $\overline{\dot{\omega}}_{S2,i} = (1/V_\Delta)(-u_{d,i}\dot{m}_d - \dot{u}_{d,i}m_d)$. The filtering operator $(\bar{\cdot})$ is used in defining the source terms because the flow field around the drop is not resolved.

3. Single drop evaporation experiments

Testing is performed with the aid of two experimental data sets. These experiments consider single drops of decane and heptane evaporating in heated, low Reynolds number environments.

The first set of experiments is from Wong & Lin (1992) and examines the evaporation of a single decane drop with an initial temperature of $T_{d,0} = 315$ K and an initial diameter of $d_{d,0} = 2.0 \times 10^{-3}$ m. The temperature of the ambient gas surrounding the drop is $\widetilde{T}_g = 1000$ K. The ambient pressure is 1 atmosphere. The drop is suspended in a convective flow with an initial Reynolds number of $\mathrm{Re}_{d,0} = 17$.

The second set of experiments is from Nomura *et al.* (1996) and examines the evaporation of a single stationary heptane drop with an initial temperature of $T_{d,0} = 298$ K and an initial diameter of $d_{d,0} = 7.0 \times 10^{-4}$ m. A range of ambient gas temperatures and pressures is studied in these experiments. Ambient temperatures range from $\widetilde{T}_g = 400$ K to $\widetilde{T}_g = 800$ K; ambient pressures range from 1 atmosphere to 50 atmospheres.

4. Parameters for sensitivity analysis

The spray model's sensitivity to a series of the parameters that appear in Eqs. (2.1)-(2.4) is studied. The studied parameters are the representative gas phase specific heat, C_p, the gas phase viscosity, μ_r, the method used to determine the drop's gas phase surface temperature, $T_{d,s}$, and the method used to determine the saturation mole fraction at the drop surface, $X_{d,s}$. Analysis is performed by conducting simulations at various ambient gas temperatures and pressures. Table 1 lists the conditions associated with each simulated case. The varies label denotes that a parameter is being changed within a particular case study. Values of the variable parameters are selected by considering the range of C_p, μ_r, $T_{d,s}$, and $X_{d,s}$ that might reasonably approximate values in the modeled system. The details of these variations are now discussed.

All thermodynamic properties are recalculated at every time step of the drop simulations. The specific heat C_p that appears in Eq. (2.4) is calculated using a standard mass fraction weighting (Miller *et al.* 1998),

$$C_p = (Y_{ref})C_{p,f} + (1 - Y_{ref})C_{p,g}, \tag{4.1}$$

where $C_{p,f}$ is the specific heat of pure fuel in the gas phase, and $C_{p,g}$ is the specific heat of the ambient gas. The ambient gas is taken to be either air or pure N_2, depending on the case being considered. The Y_{ref} parameter can be weakly interpreted as the mass fraction

Case #	Liquid fuel	Ambient temp [K]	Spray evap. model	Y_{ref} used to set C_p	T_{ref} used to set C_p	X_{ref} used to set μ_r	$X_{d,s}$ used to set B_M	Press. (atm)
1	Heptane	471	$T_{d,s}$=T_d	varies	1/3 rule	1/3 rule	Cl.-Clap.	1
2	Heptane	741	$T_{d,s}$=T_d	varies	1/3 rule	1/3 rule	Cl.-Clap.	1
3	Decane	1000	$T_{d,s}$=T_d	varies	1/3 rule	1/3 rule	Cl.-Clap.	1
4	Heptane	471	$T_{d,s}$=T_d	1/3 rule	varies	1/3 rule	Cl.-Clap.	1
5	Heptane	741	$T_{d,s}$=T_d	1/3 rule	varies	1/3 rule	Cl.-Clap.	1
6	Heptane	471	$T_{d,s}$=T_d	1/3 rule	1/3 rule	varies	Cl.-Clap.	1
7	Heptane	741	$T_{d,s}$=T_d	1/3 rule	1/3 rule	varies	Cl.-Clap.	1
8	Decane	1000	$T_{d,s}$=T_d	1/3 rule	1/3 rule	varies	Cl.-Clap.	1
9	Decane	1000	varies	1/3 rule	1/3 rule	1/3 rule	Cl.-Clap.	1
10	Heptane	746	$T_{d,s}$=T_d	1/3 rule	1/3 rule	1/3 rule	varies	5
11	Heptane	746	$T_{d,s}$=T_d	1/3 rule	1/3 rule	1/3 rule	varies	20

TABLE 1. Parameters associated with the drop simulation cases.

of fuel in the gas at the drop surface, $Y_{d,s}$ from Eq. (2.10). There is ambiguity associated with this interpretation, however, because the drop heat transfer term in Eq. (2.3) treats the ambient gas at the temperature $\widetilde{T}_g$ as a source of heat. In typical under-resolved LES settings, $\widetilde{T}_g$ will differ from the temperature at the drop surface, $T_{d,s}$. The specific heat $C_{p,g}$ that appears in the heat transfer term might then be interpreted as representative of the average gas-phase field around the drop, rather than of the field at the drop surface. Y_{ref} would then also be representative of the fuel mass fraction in the average gas-phase field. Ambiguities such as these have been noted by Law & Law (1976) and Hubbard *et al.* (1975).

To understand the influence that the specific heat calculation has on evaporation, three values of Y_{ref} will be used to set C_p in the drop simulations. These values are

(*a*) $Y_{ref} = (2/3)Y_{d,s} + (1/3)\widetilde{Y}_f$,
(*b*) $Y_{ref} = 0$,
(*c*) $Y_{ref} = 1$.

The first of these values represents the 1/3 rule that is discussed by several authors (Law & Law 1976; Hubbard *et al.* 1975). The second and third values correspond to the use of pure ambient properties or pure fuel properties, respectively.

Once Y_{ref} is calculated, the temperature at which $C_{p,f}$ and $C_{p,g}$ are evaluated must also be determined. Both of these specific heats will be calculated at a reference temperature T_{ref}. Just as with Y_{ref}, three methods of calculating T_{ref} will be employed:

(*a*) $T_{ref} = (2/3)T_d + (1/3)\widetilde{T}_g$,
(*b*) $T_{ref} = T_{b,atm}$,
(*c*) $T_{ref} = T_d$.

The first of these methods is another example of the 1/3 rule. The others test how the minimum and maximum temperatures expected at the drop surface influence results. After T_{ref} is determined, $C_{p,f}(T_{ref})$ and $C_{p,g}(T_{ref})$ are calculated using polynomial fits for each species taken from the NIST web book (NIST 2011). Diverse commentaries on these methods can be found. For example, Hubbard *et al.* (1975) suggest that the use of the 1/3 rule is best, whereas Miller *et al.* (1998) suggest using a constant wet bulb temperature for T_{ref}.

The gas viscosity μ_r is also tested for sensitivity. This viscosity affects drop evolution primarily through its influence on the τ_d parameter, which is a governing timescale in

both the drop temperature and mass equations. The same ambiguities that were present in the specification of C_p are again present in the specification of this viscosity. Unlike C_p, however, μ_r will be computed according to the semi-emperical Wilke rule,

$$\mu_r = \left(\frac{X_{ref}}{X_{ref} + (1 - X_{ref})\Omega_{f,g}}\right)\mu_f + \left(\frac{1 - X_{ref}}{X_{ref}\Omega_{g,f} + (1 - X_{ref})}\right)\mu_g, \tag{4.2}$$

$$\Omega_{f,g} = \frac{(1 + (\mu_f/\mu_g)^{1/2}(W_g/W_f)^{1/4})^2}{(8(1 + W_f/W_g))^{1/2}}, \tag{4.3}$$

where the f subscript represents fuel vapor and the g subscript represents the ambient gas vapor. Three descriptions of the reference mole fraction X_{ref} are tested,

(a) $X_{ref} = (2/3)X_{d,s} + (1/3)\widetilde{X}_f$,
(b) $X_{ref} = 0$,
(c) $X_{ref} = 1$.

Once X_{ref} is known, the μ_f and μ_g values in Eq. (4.3) are calculated using a reference temperature determined from the 1/3 rule, $T_{ref} = (2/3)T_d + (1/3)\widetilde{T}_g$. Viscosity data describing μ_f and μ_g as a function of temperature are taken from NIST web book polynomial curve fits (NIST 2011).

The final two parameters that are studied for sensitivity are the method used to calculate the gas-phase drop surface temperature, $T_{d,s}$, and the method used to calculate the saturation mole fraction, $X_{d,s}$. As shown in Table 1, case 9 considers how evaporation changes when $T_{d,s}$ is calculated using variations of the $B_M = B_T$ relationship instead of the $T_d = T_{d,s}$ relationship. Cases 10 and 11 then study the accuracy of the Clausius-Clapeyron relationship that is used to arrive at Eq. (2.11). As shown in Table 1, these cases compare the saturation mole fractions from Clausius-Clapeyron with saturation mole fractions from NIST web book data (NIST 2011). They additionally test the performance of the spray model under the type of higher pressure conditions that are expected in many engine environments.

5. Results: thermodynamic property dependencies

Results from drop simulations that investigate thermodynamic property sensitivities are shown in Figures 1 through 5. Figure 1 compares the results of heptane drop simulations at two ambient temperatures when the method used to calculate the reference mass fraction Y_{ref} appearing in the expression for C_p is varied. Figure 2 shows the corresponding data for a decane drop in an even hotter environment. The data indicate that as the reference state shifts between pure fuel and pure ambient values, the evaporation rate changes significantly. This relationship between the specified gas composition and the evaporation rate is highly dependent on the details of the individual specific heats. At the higher ambient temperature shown in the right plot of Figure 1, accounting for more fuel vapor (dashed line) tends to increase evaporation. At the lower ambient temperature shown in the left plot, accounting for more fuel vapor (dashed line) tends to slow evaporation. In the high temperature decane fuel case (Figure 2), accounting for more fuel vapor again slows evaporation. Physically, these trends are the result of the differential between $C_{p,g}$ and $C_{p,f}$ being a function of both fuel and temperature. The plots in Figure 1 and Figure 2 generally support the conclusion of Hubbard *et al.* (1975) that the 1/3 rule is acceptably accurate. The temperature profile in Figure 2, however, fails to reach the experimentally determined saturation value regardless of how C_p is specified.

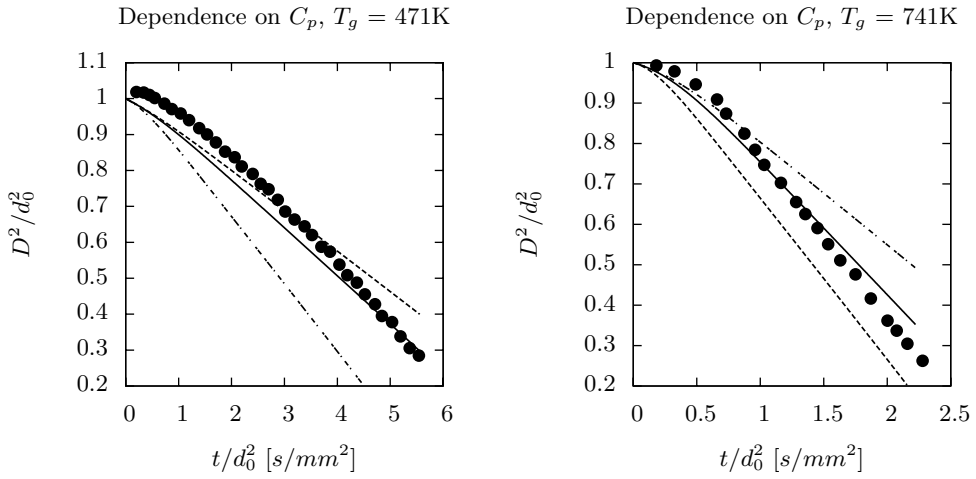

FIGURE 1. Cases 1 (left) and 2 (right). Sensitivity of heptane drop diameter (D) to the gas composition used to evaluate C_p. Experiments from Nomura *et al.* (1996) (• • •) are compared with model solutions in which C_p is evaluated as $C_p = Y_{ref}C_{p,f} + (1 - Y_{ref})C_{p,g}$ using a gas composition of $Y_{ref} = (2/3)Y_{d,s} + (1/3)\widetilde{Y}_f$ (——), $Y_{ref} = 0$ (– – –), or $Y_{ref} = 1$ (· – ·).

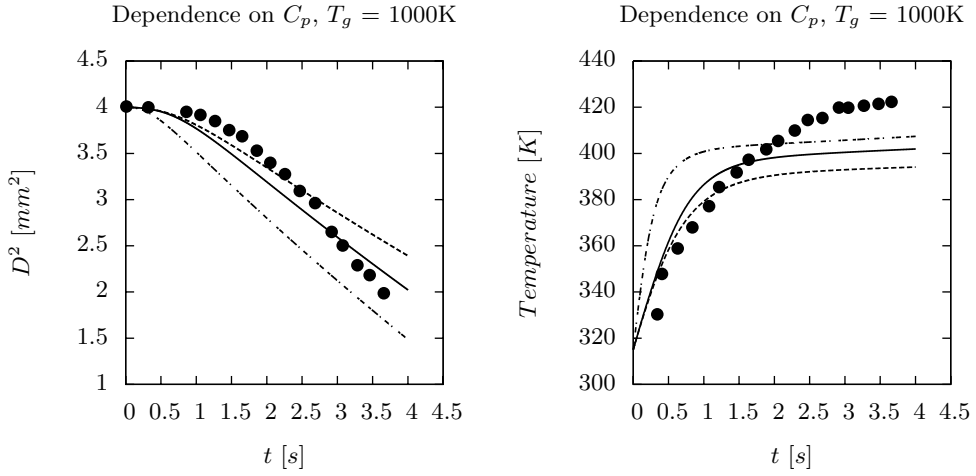

FIGURE 2. Case 3. Sensitivity of decane drop diameter (left) and drop temperature (right) to gas composition used to evaluate C_p. Experiments from Wong & Lin (1992) (• • •) are compared with model solutions in which C_p is evaluated as $C_p = Y_{ref}C_{p,f} + (1 - Y_{ref})C_{p,g}$ using a gas composition of $Y_{ref} = (2/3)Y_{d,s} + (1/3)\widetilde{Y}_f$ (——), $Y_{ref} = 0$ (– – –), or $Y_{ref} = 1$ (· – ·).

Figure 3 compares the results of heptane drop simulations at different ambient temperatures when the method used to calculate the reference temperature for C_p is varied. These data show that the specification of the reference temperature has little influence on the model when the ambient temperature is low (left plot in Figure 3), but becomes important at higher temperatures (right plot in Figure 3). This dependence can also be explained simply. At low ambient temperatures, both the boiling temperature $T_{b,atm}$ and the drop temperature T_d are reasonably close to the ambient temperature $\widetilde{T}_g$. As

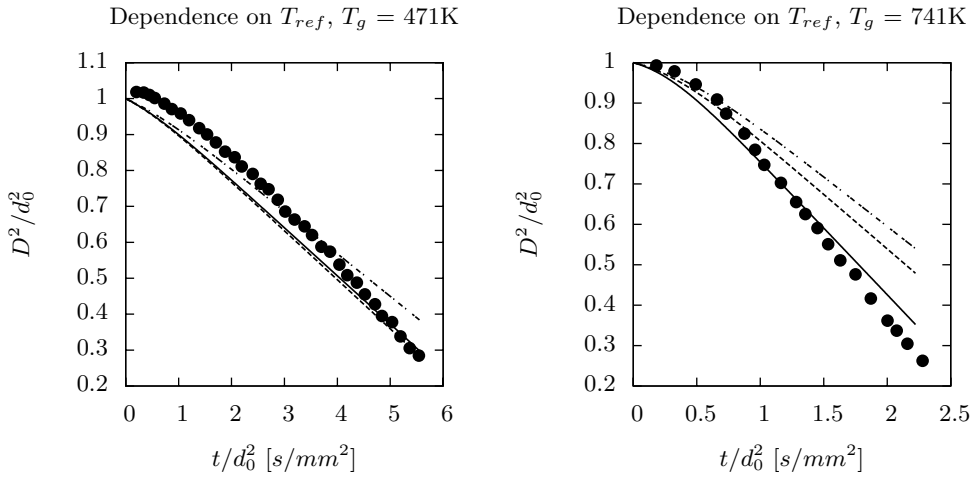

FIGURE 3. Cases 4 (left) and 5 (right). Sensitivity of heptane drop diameter (D) to the temperature used to evaluate C_p. Experiments from Nomura *et al.* (1996) (• • •) are compared with model solutions in which C_p is calculated at a temperature of $T_{ref} = (2/3)T_d + (1/3)\widetilde{T}_g$ (——); $T_{ref} = T_{b,atm}$ (– – –); $T_{ref} = T_d$ (· – ·).

$\widetilde{T}_g$ increases, neither T_b nor T_d are able to account for how the representative value of C_p changes in response. The 1/3 rule, which incorporates information about the ambient, does account for this change. Consequently, this method of specifying the reference temperature performs most accurately in the higher temperature case in Figure 3.

Figures 4 and 5 compare the results of heptane and decane drop simulations at different ambient temperatures when the method used to calculate the reference mole fraction for μ_r is varied. μ_r has a larger influence on evaporation than does C_p because the viscosity appears in the time constant τ_d that influences both drop heat transfer and drop evaporation. Figure 4 indicates that a viscosity based on pure fuel (dot dash line) leads to a strong under-prediction of evaporation, whereas a viscosity based on pure air (dashed line) leads to a moderate over-prediction of evaporation. Use of the 1/3 rule (solid line) moderates these errors, and leads to reasonable agreement with the experiments. The temperature plots in Figure 5 again fail to predict the saturation drop temperature regardless of how μ_r is calculated.

6. Results: drop surface temperature dependencies

Results from drop simulations that investigate different methods of calculating $T_{d,s}$ are shown in Figure 6. The solid lines in the figure show simulations in which it is assumed that the liquid drop temperature and the gas phase drop surface temperature are equal: $T_{d,s} = T_d$. The dot-dash lines show results in which it is assumed that $B_M = B_T$ (Eq. (2.14)), whereas the dashed lines show results in which it is assumed that $(1 + B_M)^{\phi} = (1 + B_T)$ (Eq. (2.13)). These model choices have a very strong influence on evaporation. The use of the $B_M = B_T$ equation reduces the number of assumptions in the spray model because it eliminates the need to assume that $T_{d,s} = T_d$. Incorporation of this additional information from the B_T parameter can increase the agreement between the model and the experiments, but only if used correctly. Figure 6, for example, demonstrates that both the drop diameter and the drop temperature are significantly

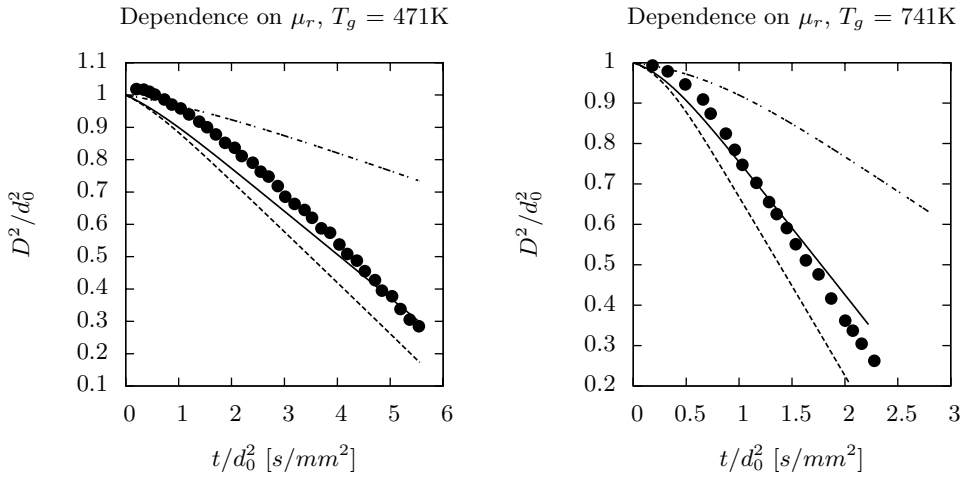

FIGURE 4. Cases 6 (left) and 7 (right). Sensitivity of heptane drop diameter to the temperature used to evaluate μ_r. Experiments from Nomura *et al.* (1996) (• • •) are compared with model solutions in which μ_r is calculated at a reference mole fraction of $X_{ref} = (2/3)X_{d,s} + (1/3)\widetilde{X}_f$ (——); $X_{ref} = 0$ (– – –); $X_{ref} = 1$ (· – ·).

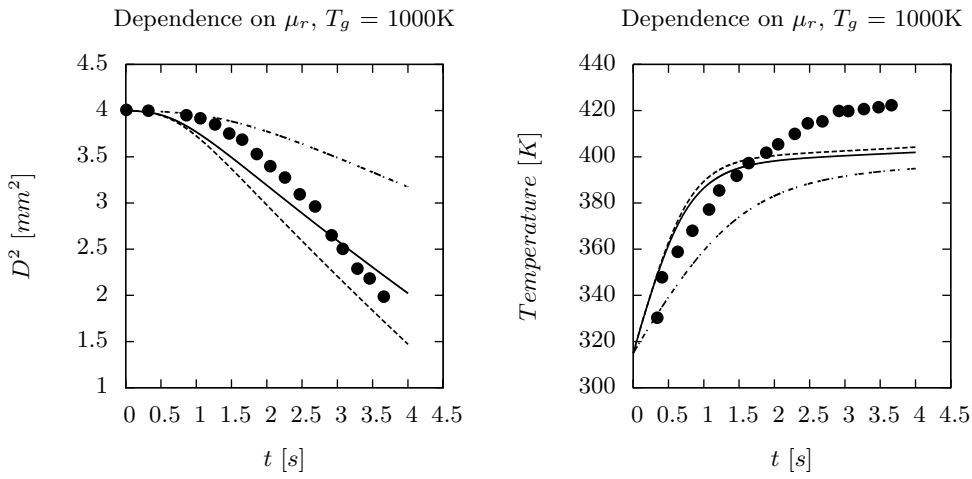

FIGURE 5. Case 8. Sensitivity of decane drop diameter (left) and drop temperature (right) to the temperature used to evaluate μ_r. Experiments from Wong & Lin (1992) (• • •) are compared with model solutions in which μ_r is calculated at a reference mole fraction of $X_{ref} = (2/3)X_{d,s} + (1/3)\widetilde{X}_f$ (——); $X_{ref} = 0$ (– – –); $X_{ref} = 1$ (· – ·).

under-predicted when the $B_M = B_T$ model is used. The under-predictions occur because because evaporation absorbs all of the heat that diffuses to the drop surface. Conversely, agreement with the experiments is much better when the model that accounts for detailed transport, $(1 + B_M)^{\phi} = (1 + B_T)$, is used. Inclusion of the specific heat ratio effectively decreases the mass flux at the surface, and the resulting model performance is seen to be in best agreement with the experimental temperature data in Figure 6.

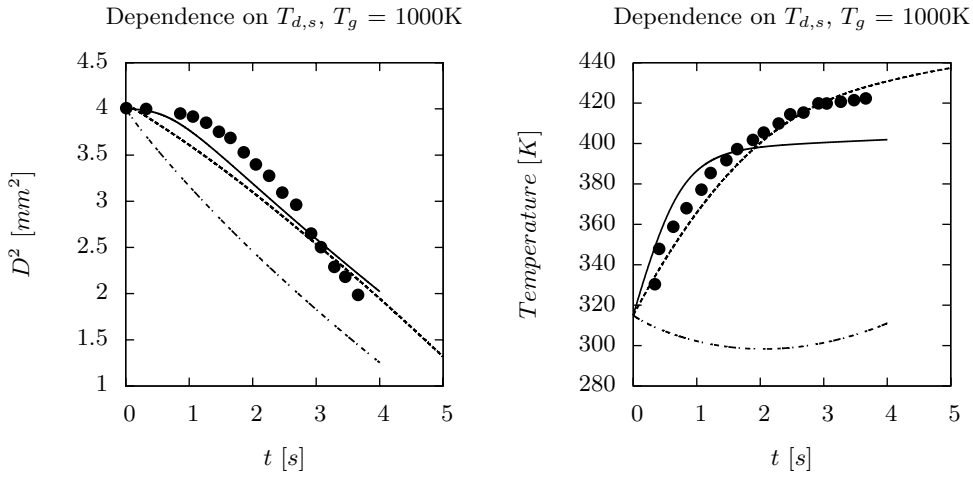

FIGURE 6. Case 9. Sensitivity of decane drop diameter to the temperature $T_{d,s}$. Experiments from Wong & Lin (1992) (• • •) are compared with model solutions in which $T_{d,s}$ is calculated by assuming $T_{d,s} = T_d$ (——), by calculating $T_{d,s}$ from Eq. (2.14) so that $B_M = B_T$ ($\cdot - \cdot$), or by calculating $T_{d,s}$ from Eq. (2.13) so that $(1 + B_M)^\phi = (1 + B_T)$ ($- - -$).

7. Results: pressure dependencies

The drop simulations that investigate pressure sensitivities are shown in Figure 7 and Figure 8. Pressure influences the drop model by changing the saturation fuel mole fraction at the drop's surface, $X_{d,s}$. When the Clausius-Clapeyron relationship is used to calculate this mole fraction, the ambient pressure P appears as a coefficient as shown in Eq. (2.11). The Clausius-Clapeyron relationship invokes several assumptions, however, and does not perfectly reproduce the saturation conditions.

A more accurate saturation mole fraction can be found using curve fit data from the NIST web book (NIST 2011). Figure 7 compares NIST saturation mole fractions with data from the Clausius-Clapeyron expression in Eq. (2.11). At a pressure of one atmosphere (atm), the Clausius-Clapeyron expression agrees with the NIST data almost perfectly. At a pressure of five atm, however, the figure shows that differences appear in the predicted saturation mole fractions at higher temperatures. At pressures above 20 atm, the Clausius-Clapeyron relation is only accurate where the drop surface temperature is low. The discrepancies at higher surface temperatures emphasize that more accurate descriptions of saturation conditions may be needed at high pressures.

Figure 8 compares the results of heptane drop simulations at ambient pressures of 5 atm (left) and 20 atm (right) when the method used to calculate the saturation mole fraction $X_{d,s}$ is varied. The left plot in Figure 8 shows no difference when the NIST web book data (NIST 2011) is used in place of the Clausius-Clapeyron equation. At pressures of 5 atm, the discrepancies that are visible in Figure 7 are too insignificant to affect evaporation. In the 20 atm environment shown on the right side of Figure 7, differences due to the saturation mole fraction start to appear. These differences are small, however, and are not responsible for the model's significant disagreement with experiments. The insensitivity to the $X_{d,s}$ calculation is attributable to evaporation being nearly complete by the time the surface temperatures reach the point where Clausius-Clapeyron and the

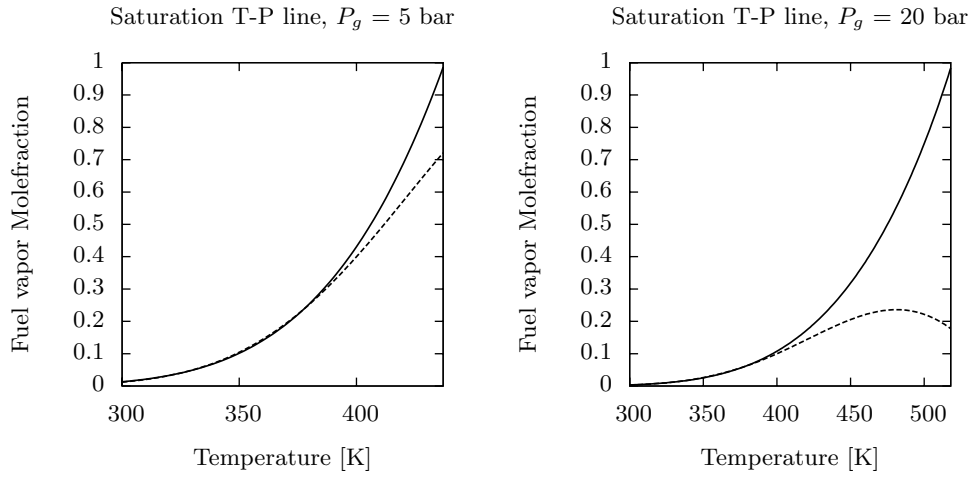

FIGURE 7. Performance of the Clausius-Clapeyron approximation. The saturation fuel mole fraction that is calculated from the saturation pressure in the NIST web book (——) is compared with the saturation fuel mole fraction calculated from the Clausius-Clapeyron expression in Eq. (2.11) ((– – –).

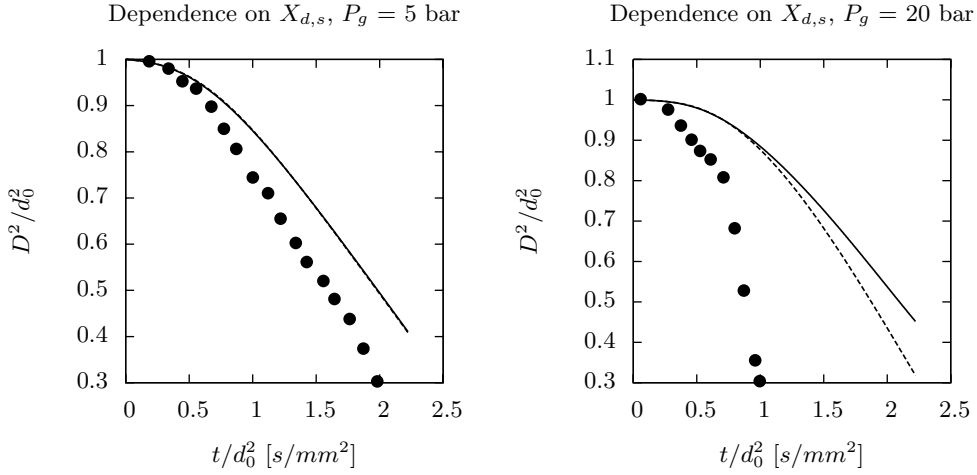

FIGURE 8. Cases 10 (left) and 11 (right). Sensitivity of heptane drop diameter to the saturation mole fraction $X_{d,s}$ used in evaluating B_M. Experiments from Nomura *et al.* (1996) (• • •) are compared with model solutions where $X_{d,s}$ is taken from Clausius-Clapeyron in Eq. (2.11) (——) or directly from the NIST web book saturation pressure (– – –).

NIST data deviate. Additional work is needed to identify the cause of these high pressure errors.

8. Summary

This study examined the sensitivities of a standard model for spray evaporation. It was determined that the calculation of thermodynamic properties such as the specific heat

capacity and the viscosity play important roles in determining evaporation. Comparisons with single drop experiments inspired suggestions regarding how these calculations should be performed. Agreement with higher pressure experimental data and drop temperature data was difficult to achieve, however, and warrants further investigation.

Acknowledgments

Support from the US Air Force Office of Scientific Research (AFOSR), the National Aeronautics and Space Administration (NASA), and the Robert Bosch Corporation is gratefully acknowledged.

REFERENCES

Baba, Y. & Kurose, R. 2008 Analysis and flamelet modelling for spray combustion. *J. Fluid Mech.* **612**, 45–79.

Crowe, C., Sommerfield, M. & Tsuji, Y. 1998 *Multiphase flows with droplets and particles*. Boca Raton, FL: CRC Press.

Faeth, G. M. 1987 Mixing, transport and combustion in sprays. *Prog. Energy Comb. Sci.* **13**, 293–345.

Hubbard, G. L., Denny, V. E. & Mills, A. F. 1975 Droplet evaporation: effects of transients and variable properties. *Int. J. Heat Mass Transfer* **18**, 1003–1008.

Knudsen, E. & Pitsch, H. 2010 Large-eddy simulation of a spray combustor using a multi-regime flamelet approach. In *CTR Ann. Res. Briefs*. Stanford University.

Law, C. K. & Law, H. K. 1976 Quasi-steady diffusion flame theory with variable specific heats and transport coefficients. *Combust. Sci. Tech.* **12** (4-6), 207–216.

Miller, R. S. & Bellan, J. 1999 Direct numerical simulation of a confined three-dimensional gas mixing layer with one evaporating hydrocarbon-droplet-laden stream. *J. Fluid Mech.* **384**, 293–338.

Miller, R. S., Harstad, K. & Bellan, J. 1998 Evaluation of equilibrium and non-equilibrium evaporation models for many-droplet gas-liquid flow simulations. *Int. J. Multiphase Flow* **24**, 1025–1055.

Nakamura, M., Akamatsu, F., Kurose, R. & Katsuki, M. 2005 Combustion mechanism of liquid fuel spray in a gaseous ame. *Phys. Fluids* **17** (123301), 1–14.

NIST 2011 http://webbook.nist.gov/chemistry/. In *NIST Chemistry WebBook, NIST Standard Reference Database* (ed. P. J. Linstrom & W. G. Mallard).

Nomura, H., Ujiie, Y., Rath, H. J., Sato, J. & Kano, M. 1996 Experimental study on high-pressure droplet evaporation using microgravity conditions. *Proc. Comb. Inst.* **26** (1), 1267–1273.

Okong'o, N. A. & Bellan, J. 2004 Consistent large-eddy simulation of a temporal mixing layer laden with evaporating drops. Part 1. Direct numerical simulation, formulation and *a priori* analysis. *J. Fluid Mech.* **499**, 1–47.

Reveillon, J. & Vervisch, L. 2005 Analysis of weakly turbulent dilute-spray ames and spray combustion regimes. *J. Fluid Mech.* **537**, 317–347.

Sazhin, S. S. 2006 Advanced models of fuel droplet heating and evaporation. *Prog. Energy Combust. Sci.* **32**, 162–214.

Wong, S. C. & Lin, A. R. 1992 Internal temperature distributions of droplets vaporizing in high-temperature convective flows. *J. Fluid Mech.* **237**, 671–687.